

Floquet driven long-range interactions induce super-extensive scaling in quantum battery

Stavya Puri^{1,2}, Tanoy Kanti Konar², Leela Ganesh Chandra Lakkaraju^{2,3}, Aditi Sen(De)²

¹ *Department of Physics, Birla Institute of Technology and Science - Pilani, Rajasthan 333031, India*

² *Harish-Chandra Research Institute, A CI of Homi Bhabha National Institute, Chhatnag Road, Jhansi, Allahabad - 211019, India and*

³ *Pitaevskii BEC Center and Department of Physics, University of Trento, Via Sommarive 14, I-38123 Trento, Italy*

Achieving quantum advantage in energy storage and power extraction is a primary objective in the design of quantum-based batteries. We explore how long-range (LR) interactions in conjunction with Floquet driving can improve the performance of quantum batteries, particularly when the battery is initialized in a fully polarized state. In particular, we exhibit that by optimizing the driving frequency, the maximum average power scales super extensively with system-size which is not achievable through next-nearest neighbor interactions or traditional unitary charging, thereby gaining *genuine quantum advantage*. We illustrate that the inclusion of either two-body or many-body interaction terms in the LR charging Hamiltonian leads to a scaling benefit. Furthermore, we discover that a super-linear scaling in power results from increasing the strength of interaction compared to the transverse magnetic field and the range of interaction with low fall-off rate, highlighting the advantageous role of long-range interactions in optimizing quantum battery charging.

I. INTRODUCTION

The development and miniaturization of technology in the modern day have led to the creation of quantum thermal devices, such as batteries [1–3], refrigerators [4], transistors [5], and heat engines [6, 7], which can outperform their classical counterparts by leveraging quantum mechanical principles. In addition to their technological implications, these studies of quantum thermal devices contribute to advancing thermodynamic concepts in the microscopic and nanoscale regimes [8].

In this work, we will focus on the benefits of developing batteries based on quantum mechanics, composed of quantum states that store and extract energy. One key factor of quantum batteries (QB) is the use of *collective operations* during the charging process. These operations can generate quantum correlations or other forms of quantumness that lead to super-extensive scaling of power (meaning that the power output increases super-linearly with the number of cells in the battery) [3, 9], known as *genuine quantum advantage* [10]. On the other hand, the quantum interacting spin models as quantum batteries have been shown to offer advantages over non-interacting models in generating power since the latter cannot create quantum correlations in the system [11–14]. However, it is necessary to note that not all collective interactions yield a genuine quantum advantage; rather, only when the norm of charging Hamiltonian increases super-extensively with system size [9, 15]. Since the concept of QBs was first proposed [1], several theoretical protocols have been developed to explore their performance, highlighting how quantum mechanical phenomena [15–37] — such as indefinite causal order [38] and many-body localization [39, 40] — can improve energy storage. These ideas have been demonstrated in various physical systems, including quantum dots [41], transmons [42–44], organic semiconductors [45], and nuclear magnetic resonance [46].

Our primary goal here is to enhance the performance of the quantum batteries by involving Floquet driving and long-range (LR) interactions into the charging process. In recent years, Floquet or time-periodic driving, also referred to as *Floquet engineering*, has emerged as a vital tool for exploring

unique characteristics in many-body systems that are typically inaccessible in equilibrium conditions (for details, see reviews [47–49]). Notable examples include topological order [47], prethermalization region [48, 50], dynamical localization and stabilization [51] and the creation of artificial magnetic fields [52, 53].

Furthermore, periodic driving can be easily implemented via oscillating electromagnetic radiation in experiments with cold atoms in optical lattices [48, 54] and solid state materials, thereby paving the way to the creation of systems with unique characteristics. Hence, it is natural to apply Floquet evolution towards building quantum technologies including quantum communication [55], quantum computing [56], quantum refrigerator [57], quantum transistor [58], heat engine [59, 60], and most recently quantum batteries [61]. In the case of QB, it was shown that although the effective periodic charging involves collective operations, it does not lead to super-extensive scaling of power [61].

We exhibit that this shortfall of Floquet charging in QB may be overcome by introducing long-range interactions. This approach expands the scope of benefits associated with LR spin models for various quantum information processing tasks, including quantum sensing and computation [62–66]. A primary advantage in terms of implementability is that LR interactions arise naturally in experiments with trapped ions and cold-atoms. At the same time, Floquet driving can also be implemented in these physical systems [54, 67–69]. To explore this, we begin with the initial product eigenstate of a non-interacting battery Hamiltonian and consider two types of LR XY spin models for charging, where the interaction range follows a power-law decay. One of these models involves two-body long-range interacting term while the other one contains many-body LR interactions. Notably, the latter can be solved analytically via Jordan-Wigner transformation [63, 70–76] while the former one can be handled numerically except for the special case corresponding to the Lipkin Meshkov Glick (LMG) model [77].

We illustrate analytically and numerically that while the battery’s power can be increased by competing next-nearest neighbor (NNN) interactions with nearest-neighbor (NN) ones, super-linear scaling cannot be attained, thereby indicat-

ing the deficiency in short-range interactions. We further exhibit that LR interactions, combined with periodic driving, can lead to super-linear scaling, provided that the strengths of the magnetic field and the LR interactions are appropriately calibrated, known as *genuine quantum advantage* [10]. In order to establish this, we adopt the definition of the maximum average power of the QB in which the optimization is performed over the stroboscopic time and the frequency of the Floquet charging. We discover that super-linear scaling can be accomplished for both kinds of LR interactions when the coordination number is close to its maximum and the fall-off rate of interactions is low enough to provide truly long-range.

The paper is organized in the following manner. Sec. II introduces the set-up of the quantum battery including LR charging Hamiltonian, its Floquet charging set-up and the benefits of additional NNN interactions with NN interactions in charging Hamiltonian. The super-extensive scaling of QB is reported for LR XY model in Sec. III. The performance of QB with the extended XY model which can be solved analytically is presented in Sec. IV. Sec. V includes the concluding remarks.

II. INTERPLAY BETWEEN NEAREST-NEIGHBOR AND NEXT-NEAREST NEIGHBOR INTERACTIONS WITH FLOQUET CHARGING

We establish here that although short-range interaction can be beneficial to enhance the power of the QB, super-extensive scaling can only be attained with LR interactions. More precisely, we focus here on the trade-off relation between nearest-neighbor and next-nearest neighbor interaction strengths present in the charging Hamiltonian which also depends on the stroboscopic time. Before presenting the results, let us fix the set-up for quantum battery under consideration.

Set-up for quantum battery: Protocol of Floquet charging

Quantum battery. We prepare the initial state of the quantum battery as a thermal equilibrium state, $\rho(0) = \exp(-\beta H_B)/\text{Tr}(\exp(-\beta H_B))$ where $\beta = 1/k_B T$ with k_B being the Boltzmann constant and T representing the temperature. We choose the battery Hamiltonian to be $H_B = h_z \sum_j \sigma_j^z$, where h_z is the strength of the local magnetic field, quantifying the local energy gap of each subsystem and σ^z is the z -component of the Pauli matrix. Note that when $\beta \rightarrow \infty$, $\rho(0)$ reaches to the ground state of H_B , i.e., $|\psi(t=0)\rangle = |00\dots 0\rangle$ with $|0\rangle$ being the ground state of σ^z .

Charging the battery. In order to obtain super-linear scaling of QB, we will demonstrate that the charging operation plays an important role. We incorporate *two* important components in the charging Hamiltonian of the QB, $H_{ch}(t) = H_B + H_{int}(t)$, which are different from the previous protocols known in the literature [61, 78]. These two crucial ingredients are as follows:

(1a) We choose variable-range interacting Hamiltonian as

H_{int} , given by

$$H_{int}^{LR} = \sum_{\substack{i < j \\ |i-j| \leq Z}}^{N-Z} \frac{J(t)}{\mathcal{N}|i-j|^\alpha} (\sigma_i^x \sigma_j^x + \gamma \sigma_i^y \sigma_j^y), \quad (1)$$

which is responsible to build a multi-site correlation between different subsystems of the QB. Here $J(t)$ is the time-dependent interaction strength between the spins at site, i and j with $\mathcal{N} = \sum_{r=1}^Z \frac{1}{r^\alpha}$, $r = |i-j|$, known as the Kac normalization factor [79], γ and Z represent the anisotropic factor and the coordination number, i.e., the distance between sites, i and j respectively and σ^k ($k = x, y, z$) are the Pauli matrices. We also assume a power-law functional form for the decay of the interactions with the increasing distance between the spins such that α corresponds to the fall-off rate of this power law-decay. In this case, an open-boundary is considered. By changing α values, we can have long-range interactions with $0 \leq \alpha \leq 1$, quasi LR interactions for $1 < \alpha \leq 2$ and short-range interaction when $\alpha > 2$. Note that $\alpha = 0$ corresponds to the LMG model [77]. In this work, we study the gain in QB by varying both α and Z .

(1b) Another model that we choose for charging is the extended XY model which can be solved analytically by Jordan-Wigner transformation [70–72]. In this case, the interacting Hamiltonian reads as

$$H_{int}^{exXY} = \sum_{j=1}^N \sum_{r=1}^{\frac{N}{2}} \frac{J(t)}{4\mathcal{N}r^\alpha} (\sigma_j^x \mathbb{Z}_r^z \sigma_{j+r}^x + \gamma \sigma_j^y \mathbb{Z}_r^z \sigma_{j+r}^y), \quad (2)$$

where $\mathbb{Z}_r^z = \prod_{l=j+1}^{j+r-1} \sigma_l^z$, with $\mathbb{Z}_1^z = \mathbb{I}$, with α being the strength of power-law decay and the Kac-scaling factor respectively as given in Eq. (1). Here a periodic boundary condition is considered. We are interested to find out whether the extended XY model in Eq. (2) involving both N -body interactions and long-range interactions can provide similar or any additional benefit compared to the long-range models in Eq. (1).

(2) We consider the evolution of QB through square wave with time period, $T = \frac{2\pi}{\omega}$, given as

$$J(t) = \begin{cases} +J; & nT < t < (n+1/2)T \\ -J; & (n+1/2)T < t < nT, \end{cases} \quad (3)$$

where ω represents the frequency of the periodic driving. Given the square wave form of the periodic drive performed at stroboscopic times, we use the unitary of the form

$$U_1 = \exp\left[-i(H_B + H_{int})\frac{T}{2}\right], U_2 = \exp\left[-i(H_B - H_{int})\frac{T}{2}\right], \\ U^F(T) = U_2 U_1, \quad (4)$$

where U^F is unitary corresponding to the periodic time, T . The n^{th} stroboscopic evolution from the initial state, $|\psi(t=0)\rangle$, is given as $|\psi(t=nT)\rangle = (U^F)^n |\psi(t=0)\rangle$.

Performance quantifier. In order to certify the performance of the battery with respect to its capability in storing and extractable energy, we compute the work stored in a given

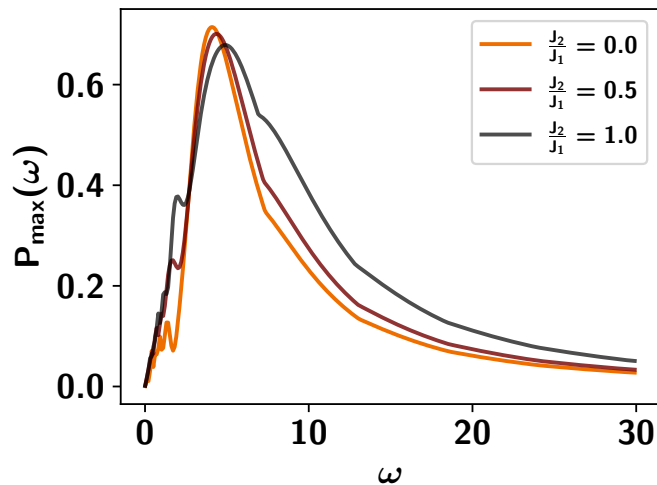


FIG. 1. Behavior of $P_{\max}(\omega)$ (ordinate) against ω (abscissa) of the XY model with the increase of J_2/J_1 (from dark to light lines). Here $h_z = 0.5$, $\gamma = -1$ and $N = 8$. The initial state is the product ground state of the battery Hamiltonian, $H_B = h_z \sum_j \sigma_j^z$. We observe that there exists ω values for which $P_{\max}(\omega)$ attain its maximum. Both the axes are dimensionless.

battery at each stroboscopic time, nT , as $W(t = nT) = \text{Tr}(H_B \rho(t)) - \text{Tr}(H_B \rho(0))$, where $\rho(0)$ and $\rho(t)$ are the initial and the evolved state of the battery. Since changing certain parameters of the Hamiltonian can cause extraction of more power, making the design unreasonable, we normalize the Hamiltonian. It makes its spectrum to be bounded by $[-1, 1]$, irrespective of any system parameters which is given as $(E_{\max} - E_{\min})^{-1}[2H_B - (E_{\max} + E_{\min})\mathbb{I}] \rightarrow H_B$.

We are interested to investigate the maximum average power of the battery at each stroboscopic time, given by

$$P_{\max}^{\omega} = \max_{n, \omega} \frac{W(nT)}{nT}, \quad (5)$$

where the maximization is performed over stroboscopic time, t and the frequency range, ω . Note that the optimization over ω does not appear in the unitary evolution and is not considered for Floquet charging in literature (see Ref. [61]). Further, when $\omega \rightarrow 0$, the system evolves unitarily and the time period is very high for which power through stroboscopic time become very small, i.e., $P_{\max} \rightarrow 0$ while for $\omega \rightarrow \infty$, QB evolves through an average Hamiltonian H_B resulting in $P_{\max} \rightarrow 0$. Therefore, it highlights that nonvanishing maximum power depends upon ω and genuine quantum advantage through Floquet charging can only be confirmed through optimization over frequency as well as stroboscopic time. In other words, we are interested to identify the favorable situation in which quantum advantage can be maximized as done in case of other quantum tasks [80–83]. Note here that the normalization of the battery Hamiltonian H_B described above is not performed when we compute the scaling behavior of P_{\max}^{ω} with the system-size N since we want to compare our results with the known results in literature computed without normalization.

A. Advantage of having NN and NNN interactions though no super-linear scaling

Before moving to the charging with LR interactions (i.e., with arbitrary α and arbitrary Z), let us first analyze whether along with nearest-neighbor interactions, denoted by J_1 , if one incorporates next-nearest neighbor interaction with J_2 in the charging Hamiltonian (i.e., $\alpha = 0$ and $Z = 2$ in Eq. (1)), any enhancement of power can be achieved or not. The Hamiltonian can be written explicitly as

$$H_{int}^{NNN} = \sum_{i=1}^{N-1} \frac{J_1(t)}{2} (\sigma_i^x \sigma_{i+1}^x + \gamma \sigma_i^y \sigma_{i+1}^y) + \sum_{i=1}^{N-2} \frac{J_2(t)}{2} (\sigma_i^x \sigma_{i+2}^x + \gamma \sigma_i^y \sigma_{i+2}^y), \quad (6)$$

To address this query, we choose two paths – (1) we study $P_{\max}(\omega) = \max_n \frac{W(nT)}{nT}$ by varying the strength of J_2/J_1 for a fixed ω and the same with the increase of ω for different values of J_2/J_1 ; (2) secondly, for a large values of ω , we apply Floquet-Magnus expansion [84] and study the scaling behavior of this model with N for various J_2/J_1 strength and try to see whether we can beat linear scaling obtained for NN interacting charging.

1. Gain in power with NNN interacting charger

We first note that power can be enhanced when charging Hamiltonian contains any kinds of interactions, thereby confirming the role of quantumness for storing energy in the battery. In case of Floquet charging, another crucial component is the frequency. To determine the role of ω and the interaction strengths, we investigate the behavior of $P_{\max}(\omega, J_2/J_1, h_z)$ where J_2/J_1 and h_z are system parameters of the QB and charger respectively. Since we are interested to explore the role NNN interactions in charging, we fix h_z to be moderately low compared to the interaction strength.

Observation 1. The entire profile of $P_{\max}(\omega, J_2/J_1)$ depends crucially on ω (see Fig. 1), showing the importance of frequency in the Floquet driving. It is evident from the investigation that for a fixed system parameters, the maximum of $P_{\max}(\omega)$ is achieved only for a single value of ω .

Observation 2. $P_{\max}(\omega, J_2/J_1)$ oscillates non-uniformly with the variation of J_2/J_1 for a fixed ω value although it saturates when J_2/J_1 is moderately high. In particular, for some values of ω , there exist a range of J_2/J_1 for which $P_{\max}(\omega, J_2/J_1) \geq P_{\max}(\omega, J_2/J_1 = 0)$, thereby illustrating the benefit of NNN interactions in charging. However, the increasing value of J_2 over J_1 is not ubiquitously beneficial as depicted in Fig. 2. It only highlights that the competition between NN and NNN interactions matters in storing energy. This observation also justifies the importance of maximizing ω for studying the power of the QB.

Observation 3. Let us consider the maximum stored energy with stroboscopic time, given by $W_{\max}(J_2/J_1, h_z) = \max_n W(nT)$ which reaches maximum for some ω values

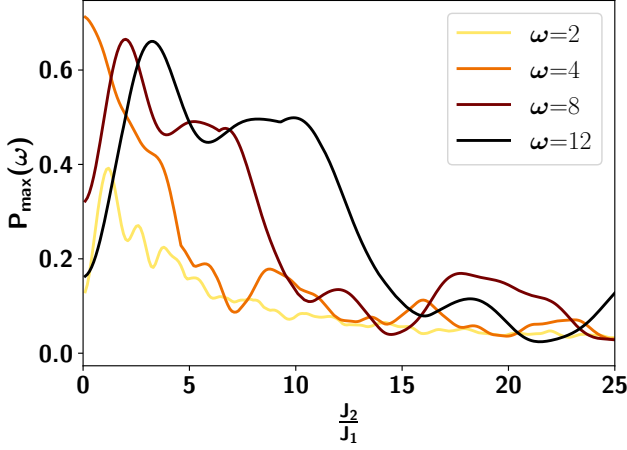


FIG. 2. $P_{\max}(\omega)$ (ordinate) with respect to $\frac{J_2}{J_1}$ (abscissa) of the XY model with the increase of the frequency of the periodic driving, ω (from light to dark lines). All the system parameters are same as in Fig. 1. Clearly, there exists ω_c above which NNN interaction combined with NN ones provides advantage over the charging Hamiltonian with only NN interactions. Both the axes are dimensionless.

when the system parameters are fixed. The ω for which W_{\max} achieves maximum changes with the ratio between the NN and NNN interactions for a weak magnetic field strength. Interestingly, we observe that with the increasing J_2/J_1 , W_{\max} increases with ω and as shown for $P_{\max}(\omega, J_2/J_1)$, there exists ω_c for a fixed J_2/J_1 which leads to the maximum of W_{\max} .

2. No benefit in scaling with NNN interactions

To perform the scaling analysis analytically, we will derive the time-independent Floquet Hamiltonian for the charging by using Floquet-Magnus expansion (FME) [47, 84, 85]. Since the charging Hamiltonian is periodic in time, i.e., $H_{ch}(t) = H_{ch}(t + T)$, we invoke Floquet theory to study the dynamics of the quantum battery. We calculate the time-independent Floquet Hamiltonian, $H_{ch}^F[t_0]$, which can be used to evolve the system at stroboscopic time periods τ ($\tau \in n(T + t_0) \forall n \in \mathbb{Z}^+$) as

$$U^F(\tau, t_0) = e^{(-iH_{ch}^F[t_0]\tau)}. \quad (7)$$

We fix $t_0 = 0$, thereby neglecting $[t_0]$ further in our calculation. To compute H_{ch}^F in the high frequency limit, i.e., when ω is high enough, we use the Floquet-Magnus expansion upto $O(T^3)$ terms and rewrite the charging Hamiltonian in Eq. (6) as

$$H_{ch}^F = H^{F_0} + H^{F_1} + H^{F_2} + H^{F_3}, \quad (8)$$

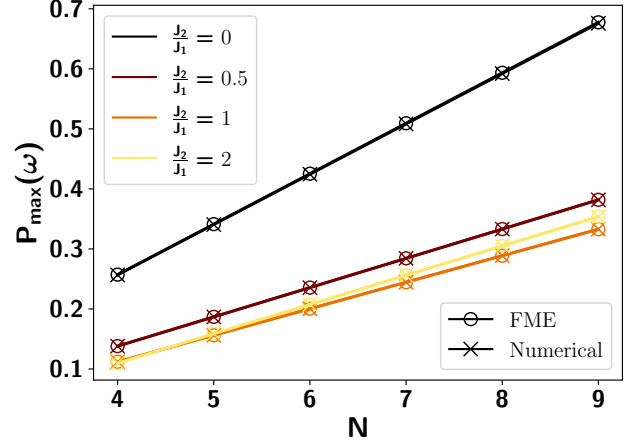


FIG. 3. **Scaling analysis for charging Hamiltonian with NN and NNN interactions.** $P_{\max}(\omega)$ (vertical axis) against N (horizontal axis). Here $\omega = 25$ and $h_z = 0.5$. Dark to light solid lines represent the increase of the values of $\frac{J_2}{J_1}$. The scaling of $P_{\max}(\omega)$ is computed both by Floquet-Magnus expansion and by numerical methods which match exactly. It is evident from the figure that $P_{\max}(\omega) \sim aN + b$ where (a, b) depends on the $\frac{J_2}{J_1}$ values. For example, for $\frac{J_2}{J_1} = 0$, $(0.084, -0.079)$; $\frac{J_2}{J_1} = 0.5$, $(0.0487, -0.0569)$; $\frac{J_2}{J_1} = 1$, $(0.044, -0.065)$; and $\frac{J_2}{J_1} = 2$, $(0.048, -0.085)$. Both the axes are dimensionless.

where

$$\begin{aligned} H^{F_0} &= \frac{H_1 + H_2}{2}, \quad H^{F_1} = -i\frac{T}{8}[H_2, H_1], \\ H^{F_2} &= -\frac{T^2}{96}[[H_2, H_1], H_1 - H_2], \\ H^{F_3} &= i\frac{T^3}{384}[H_2, [[H_2, H_1], H_1]], \end{aligned} \quad (9)$$

with

$$\begin{aligned} H_1 &= h_z \sum_j \sigma_j^z + \frac{J_1}{2} \sum_j (\sigma_j^x \sigma_{j+1}^x + \gamma \sigma_j^y \sigma_{j+1}^y) \\ &\quad + \frac{J_2}{2} \sum_j (\sigma_j^x \sigma_{j+2}^x + \gamma \sigma_j^y \sigma_{j+2}^y), \end{aligned} \quad (10)$$

$$\begin{aligned} H_2 &= h_z \sum_j \sigma_j^z - \frac{J_1}{2} \sum_j (\sigma_j^x \sigma_{j+1}^x + \gamma \sigma_j^y \sigma_{j+1}^y) \\ &\quad - \frac{J_2}{2} \sum_j (\sigma_j^x \sigma_{j+2}^x + \gamma \sigma_j^y \sigma_{j+2}^y). \end{aligned} \quad (11)$$

Using Eqs. (10) and (11) with $J_i = J'_i/2$ ($i = 1, 2$), we can explicitly write

$$\begin{aligned}
H^{F_0} &= h_z \sum_j \sigma_j^z \\
H^{F_1} &= \frac{T}{2}(1-\gamma)h_z \left[J_1 \sum_j (\sigma_j^y \sigma_{j+1}^x + \sigma_j^x \sigma_{j+1}^y), \right. \\
&\quad \left. + J_2 \sum_j (\sigma_j^y \sigma_{j+2}^x + \sigma_j^x \sigma_{j+2}^y) \right] \\
H^{F_2} &= -\frac{T^2}{3}(1-\gamma)h_z \left[(J_1^2 + J_2^2)(1-\gamma) \sum_j \sigma_j^z, \right. \\
&\quad + J_1 J_2 \sum_j (\sigma_j^z \sigma_{j+1}^x \sigma_{j+2}^x - \gamma \sigma_j^z \sigma_{j+1}^y \sigma_{j+2}^y) \\
&\quad + J_1 J_2 \sum_j (\sigma_j^x \sigma_{j+1}^x \sigma_{j+2}^z - \gamma \sigma_j^y \sigma_{j+1}^y \sigma_{j+2}^z) \\
&\quad + J_1 J_2 \sum_j (\sigma_j^x \sigma_{j+1}^z \sigma_{j+3}^x - \gamma \sigma_j^y \sigma_{j+1}^z \sigma_{j+3}^y), \\
&\quad + J_1 J_2 \sum_j (\sigma_j^x \sigma_{j+2}^z \sigma_{j+3}^x - \gamma \sigma_j^y \sigma_{j+2}^z \sigma_{j+3}^y) \\
&\quad + J_1^2 \sum_j (\sigma_j^x \sigma_{j+1}^z \sigma_{j+2}^x - \gamma \sigma_j^y \sigma_{j+1}^z \sigma_{j+2}^y) \\
&\quad \left. + J_2^2 \sum_j (\sigma_j^x \sigma_{j+2}^z \sigma_{j+4}^x - \gamma \sigma_j^y \sigma_{j+2}^z \sigma_{j+4}^y) \right],
\end{aligned}$$

and so on. For FME expansion, we consider H_{ch}^F instead of H_{ch} in Eq. (4).

Let us now investigate how $P_{\max}(\omega)$ scales with N obtained analytically using FME and by explicit numerical simulation for a high values of ω . We find that for a fixed h_z and a high ω , $P_{\max}(\omega) \sim aN + b$ where a and b are constants. We observe that the scaling with N for different J_2/J_1 values via numerical simulation exactly matches with the one obtained by using FME (see Fig. 3 with $\omega = 25$). It demonstrates that despite the presence of next-nearest neighbor term in the charging Hamiltonian, the scaling cannot be made super-extensive which indicates that SR interactions are not enough to attain super-linear scaling in power.

III. SUPER-LINEAR SCALING WITH LONG-RANGE SYSTEM VIA FLOQUET DRIVING

We now delve into the charging Hamiltonian involving long-range interactions. It was shown that the maximum power with charging being with NN interactions scales linearly through Floquet driving although Floquet charging involves effectively N -body interaction [61]. We exhibit here that a super-extensive scaling of average power can be achieved if charging is done through the long-range interacting Hamiltonian provided Floquet frequency is tuned appropriately. Interestingly,

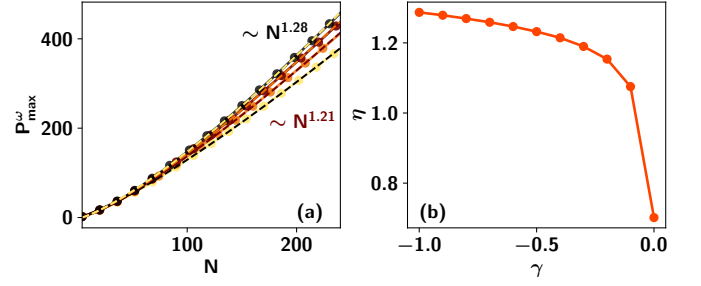


FIG. 4. **Scaling analysis for LMG charging Hamiltonian.** (a) P_{\max}^{ω} (ordinate) with system-size N (horizontal axis), when the charging Hamiltonian is the two-body LR XY model with $\alpha = 0$. By least-square fitting method, we find that it scales as $P_{\max}^{\omega} \sim aN^{\eta} + b$, where a and b are constants, with $\eta > 1$ as mentioned in the figure. (b) Dependence of η (ordinate) on γ (abscissa) which shows the scaling upto ≈ 1.3 . Other parameters are $h_z = 1$, and $J = 20$. All the axes are dimensionless.

we also show that such scaling cannot be achieved by unitary evolution.

A. Super-extensive scaling of power for LMG model

In order to show the super-linear scaling, we have to demonstrate that the maximum average power after optimizing over stroboscopic time and the driven frequency, scales as

$$P_{\max}^{\omega} \sim aN^{\eta} + b, \quad (12)$$

with the scaling exponent, $\eta > 1$ and a , and b being constants. $\eta = 1$ corresponds to the linear scaling as observed with NN interacting charging Hamiltonian and when the evolution is governed by the time-independent unitary operator [15, 86]. We will be presenting the scaling analysis in two parts – (1) LR interacting Hamiltonian with $\alpha = 0$ and $Z = N - 1$ which represents the LMG model [77]; (2) persistence of superlinear scaling for $0 \leq \alpha \leq 1$, which represents the LR XY model.

Scaling in the LMG model. For $\alpha = 0$, the LMG Hamiltonian can be represented in the angular momentum basis, reducing the dimension of the system from $2^N \times 2^N$ to $N \times N$ which show several exotic properties [87–89]. Specifically, we can rewrite the Hamiltonian as

$$\begin{aligned}
H_{int}^{LR} &= \frac{J}{2N} [(1+\gamma)(S_+ S_- + S_- S_+ - N) \\
&\quad + (1-\gamma)(S_+^2 + S_-^2)] + S_z,
\end{aligned} \quad (13)$$

where $S_l = \frac{1}{2} \sum_i \sigma_i^l$ where $l \in \{x, y, z\}$ and $S_{\pm} = S_x \pm iS_y$. Such a formalism allows us to obtain P_{\max}^{ω} for a large system-size which is not possible for $\alpha \neq 0$. We observe that when $-1 \leq \gamma \leq 0$, the scaling exponent in the maximum average power lies above unity, i.e., $1 < \eta \leq 1.5$, as depicted in Figs. 4. Eg. when $h_z/J = 0.05$ and $\gamma = -1.0$, the scaling equation reads as $P_{\max}^{\omega} = aN^{1.28} + b$ where $a = 0.39$, $b = -2.24$ and mean square error is 0.16% (see Fig. 4). It also highlights that $\gamma = -1$ is the best choice to obtain super-linear scaling compared to any values from $\gamma < 0$. This can be intuitively

understood as the norm of the commutator, i.e., $\| [H_B, H_{int}^{LR}] \|$, maximizes when $\gamma < 0$.

Competitions between magnetic field and interaction strengths in scaling and power. Let us now study how the scaling exponent, η , depends on the ratio between the strength of the magnetic field and the interaction, h_z/J . When the interaction strength dominates over the strength of the magnetic field, i.e., when $\frac{h_z}{J} \ll 1$ (in the paramagnetic phase), we observe the non-linear scaling with $\eta > 1$ while for $\frac{h_z}{J} > 1$ (in the ferromagnetic phase), the scaling remains extensive although the magnitude of P_{\max}^ω is higher than that for $h_z/J > 1$. Notice, further, that with the increase of J such that $h_z/J \ll 1$, the scaling exponent increases and, finally, it saturates to $N^{1.5}$.

Floquet vs quench driving. In the ferromagnetic phase ($\frac{h_z}{J} > 1$), the maximum average power via Floquet drive far exceeds the scaling (although non-super-extensive) and the magnitude of power while in the paramagnetic phase, opposite picture emerges. Specifically, for $\frac{h_z}{J} < 1$, P_{\max}^ω through the time-independent unitary charging is higher than that of the Floquet drive provided the system-size is moderate. For a large system-size, again Floquet-driven power becomes the best.

B. Scaling with power-law fall-off rate

We now investigate how the scaling and other behavior of P_{\max}^ω change with the increase of α . Firstly, when $\alpha \leq 2$ along with $\gamma = -1$, the numerical simulation reveals that the charging Hamiltonian in Eq. (1) in the paramagnetic phase ($h_z/J \ll 1$) continues to provide super-extensive scaling. In particular, the scaling exponent, η in Eq. (12), increases with the decrease of α (as shown in Fig. 5) and achieves its maximum when $\alpha \rightarrow 0$. This result clearly exhibits that the long range interactions (both in LR and quasi LR regimes) along with periodic driving lead to a significant increase in the scaling as opposed to the short range interactions involved in the charging Hamiltonian. This implies that the super-linear scaling is possibly related to the capability possessed by the driving Hamiltonian in terms of distributing entanglement among sites [90]. Further, we notice that when $\alpha \gg 2$, the scaling even with Floquet driving becomes linear with N . Eg. for $\alpha = 5$ and $h_z/J = 0.1$, $P_{\max}^\omega \sim aN + b$ with $a = 0.32$, and $b = 0.04$.

Response of coordination number in the scaling of the model. We have already shown that the scaling of P_{\max}^ω is super-extensive when $0 \leq \alpha \leq 2$, $\gamma < 0$ and $Z = N - 1$. Let us now ask the following question – “how does this super-linear scaling and magnitude of power depend on the range of interactions in the long-range domain?” Again, we start our analysis of the charging Hamiltonian by fixing $h_z/J \ll 1$. Firstly, the magnitude of P_{\max}^ω increases with Z for different $\alpha \leq 2$ values, belonging to LR and quasi long-range regimes and in the domain where $J \gg h_z$. In particular, as α increases, the maximum power does not change significantly with Z while for small α , especially when $\alpha < 1$, P_{\max}^ω increases monotonically with Z (see Fig. 6). This is possibly due to the fact that strong long-range interaction is capable

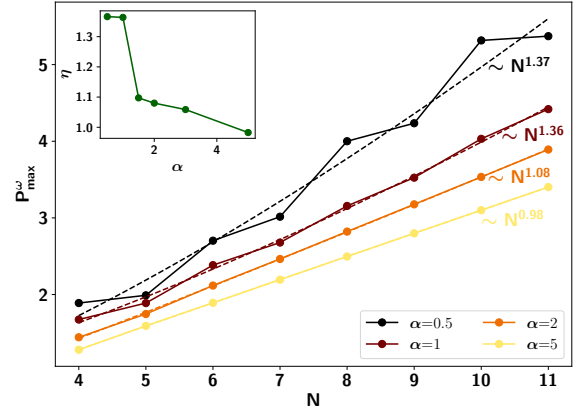


FIG. 5. **Scaling of LR XY charging Hamiltonian.** Behavior of P_{\max}^ω against system-size N with $h_z = 0.5$, $J = 5$, $\gamma = -1$. Periodic driving along with LR interaction induces super-extensive scaling, i.e., when $\alpha < 2$, $P_{\max}^\omega \sim aN^\eta + b$ with $\eta > 1$ and a, b being constants. Inset depicts how super-linear scaling exponent η (vertical axis) changes with LR interaction strength α (horizontal axis). Both the axes are dimensionless.

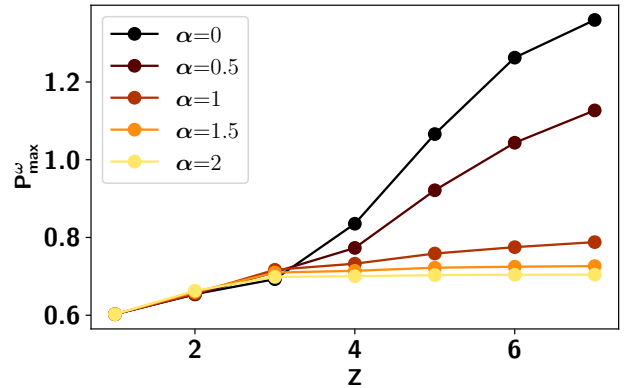


FIG. 6. P_{\max}^ω (ordinate) vs coordination number Z (abscissa) with $\gamma = -1$. Dependency upon Z is displayed for different long-range strength, α , in the long-range XY model. Other system parameters are $J = 20$, $h_z = 0.5$ and $N = 8$. Clearly, low α and high Z provides high P_{\max}^ω . Both the axes are dimensionless.

of creating high entanglement among all the sites, leading to a greater quantum advantage in QB in comparison with the nearest-neighbor or few neighbor interacting charger.

In the context of scaling, we already know two extreme cases: $Z = 2$ gives linear scaling, i.e., $\eta = 1$ as shown in Sec. II while $Z = N - 1$, $\eta = 1.5$ with $\alpha \leq 2$. It is evident from Fig. 7 that with the increase of Z , the scaling exponent, η , increases.

IV. SCALING WITH EXTENDED XY MODEL

In order to compute the average maximum power with the charging being the extended XY model in Eq. (2), we first

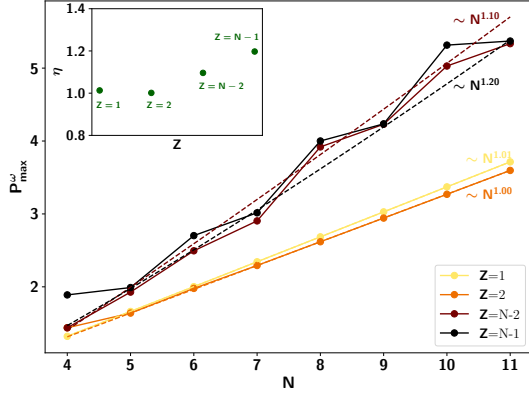


FIG. 7. **Scaling of P_{\max}^{ω} (ordinate) vs system-size N (abscissa) with $\gamma = -1$ and $\alpha = 0.5$.** Dependency upon N is displayed for different coordination number Z in the long-range XY model. Other system parameters are $J = 5$, $h_z = 0.5$ and $N = 8$. Inset displays η (vertical axis) with respect to Z (horizontal axis). It clearly indicates the influence of Z on achieving super-extensive scaling in P_{\max}^{ω} as η increases with Z . All the axes are dimensionless.

rewrite the Hamiltonian in the fermionic basis following the Jordan-Wigner transformation [70–72, 91] as

$$\begin{aligned}\sigma_n^x &= (c_n + c_n^\dagger) \prod_{m < n} (1 - 2c_m^\dagger c_m), \\ \sigma_n^y &= i (c_n - c_n^\dagger) \prod_{m < n} (1 - 2c_m^\dagger c_m), \\ \text{and } \sigma_n^z &= 1 - 2c_n^\dagger c_n,\end{aligned}\quad (14)$$

where c_m^\dagger (c_m) is the creation (annihilation) operator of spinless fermions and they follow fermionic commutator algebra. The Hamiltonian in such basis reads as

$$\begin{aligned}H_{int}^{extXY} &= \sum_n \sum_r \frac{J_r(t)}{2} [(1 + \gamma)c_n^\dagger c_{n+r} + (1 - \gamma)c_n^\dagger c_{n+r}^\dagger \\ &+ \text{h.c.}]\end{aligned}\quad (15)$$

We prepare the initial state as the ground state of $H_B = \frac{h_z}{2} \sum_j \sigma_j^z$ and it is evolved through $H_{ch} = H_B + H_{int}^{extXY}$ which can be mapped to a quadratic free fermionic model given in Eq. (15). To compute the power of the battery, we rewrite the charging Hamiltonian in the momentum space by performing a Fourier transform of $c_n = \frac{1}{\sqrt{N}} \sum e^{-i\phi_k} c_k$ where $\phi_k = \frac{(2k-1)\pi}{N} \forall k \in \pm[1, N/2]$ (we consider periodic boundary condition for this integrable model) and in this space, the model is described as $H_{int}^{extXY} = \bigoplus_{k \geq 0} \Psi_k H_k \Psi_k^\dagger$ where

$$H_k = \begin{bmatrix} \text{Re}(J_k^\alpha(t))(1 + \gamma) - h_z & i\text{Im}(J_k^\alpha(t))(1 - \gamma) \\ -i\text{Im}(J_k^\alpha(t))(1 - \gamma) & -\text{Re}(J_k^\alpha(t))(1 + \gamma) + h_z \end{bmatrix}, \quad (16)$$

with $J_k^\alpha = \sum_{r=1}^{\frac{N}{2}} J_r e^{i\phi_k r}$ and $\Psi_k^\dagger = (c_k \quad c_{-k}^\dagger)$ being the Bogoliubov basis. Hence, the effective unitary that can describe the stroboscopic evolution of QB for each mode k is given as

$$\begin{aligned}U_k &= \exp\left(-iH_k(-J)\frac{T}{2}\right) \exp\left(-iH_k(+J)\frac{T}{2}\right) \\ &= \exp(-H_k^F T),\end{aligned}\quad (17)$$

where H_k^F is the Floquet Hamiltonian. This Hamiltonian can be evaluated since $H_k^F = \sum_{k \geq 0} \beta_T(k) \vec{n}_k \cdot \vec{\sigma}_k$ with $\vec{n}_k = \frac{1}{\sqrt{1-u_k^0}} [u_k^x, u_k^y, u_k^z]$ and $\beta_T(k) = \frac{1}{T} \cos^{-1} u_k^0$. Here $\vec{\sigma}_k$ are the Pauli matrices in the Bogoliubov basis. The elements of \vec{n}_k read as

$$\begin{aligned}u_k^0 &= \cos\left(\frac{E_k^1 T}{2}\right) \cos\left(\frac{E_k^2 T}{2}\right) \\ &\quad - \cos(\Delta_k) \sin\left(\frac{E_k^2 T}{2}\right) \sin\left(\frac{E_k^1 T}{2}\right), \\ u_k^x &= \sin\left(\frac{E_k^1 T}{2}\right) \sin\left(\frac{E_k^2 T}{2}\right) \sin(\Delta_k), \\ u_k^y &= \cos\left(\frac{E_k^1 T}{2}\right) \sin\left(\frac{E_k^2 T}{2}\right) \sin(\theta_k^2) \\ &\quad + \cos\left(\frac{E_k^2 T}{2}\right) \sin\left(\frac{E_k^1 T}{2}\right) \sin(\theta_k^1), \\ u_k^z &= -\cos\left(\frac{E_k^1 T}{2}\right) \sin\left(\frac{E_k^2 T}{2}\right) \cos(\theta_k^2) \\ &\quad - \cos\left(\frac{E_k^2 T}{2}\right) \sin\left(\frac{E_k^1 T}{2}\right) \cos(\theta_k^1),\end{aligned}\quad (18)$$

where $E_k^i = \sqrt{(\text{Re}(J_k^\alpha)_i - h_z)^2 + \text{Im}(J_k^\alpha)_i^2}$, $\cos(\theta_k^i) = (\text{Re}(J_k^\alpha)_i - h_z)/E_k^i$ with $i \in \{1, 2\}$ and $\Delta_k = \theta_k^1 - \theta_k^2$.

Therefore, the energy stored in the QB at the n^{th} stroboscopic time can be analytically obtained as $W(nT) = \sum_{k \geq 0} \langle 0_k | (U_k^\dagger)^n H_{B,k} (U_k)^n | 0_k \rangle - \langle 0_k | H_{B,k} | 0_k \rangle$ with $|0_k\rangle$ is the initial state and $H_{B,k} = -h_z \sigma_k^z$ is the battery Hamiltonian in the momentum space. The work output takes the form as

$$W(nT) = \sum_{k \geq 0} 2h_z (1 - (n_k^z)^2) \sin^2(n \cos^{-1} u_k^0). \quad (19)$$

It is evident from the above expression that the work in the stroboscopic time depends nonlinearly on the frequency of the Floquet driving, $T = 2\pi/\omega$. Clearly, it is a function of ω , α , h_z and J , i.e., $f(\alpha, \omega, h_z, J)$ which indicates that by calibrating ω , α and h_z/J , we can obtain nonlinear scaling in the maximum average power, P_{\max}^{ω} with system-size as presented in Fig. 8. The figure illustrates that $P_{\max}^{\omega} \sim aN^\eta + b$, with $\eta > 1$ when we are in deep long-range regime with $0 \leq \alpha < 1$. It again establishes the genuine quantum advantage of long-range interactions during charging of the QB through Floquet driving. However, super-extensive scaling, in this case, cannot be accomplished in the quasi long-range domain ($1 < \alpha < 2$) which is, in contrast, to the LR XY model presented in Sec. III.

V. CONCLUSION

Floquet engineering has become a useful tool to showcase several exotic phenomenon in physical systems. With the development of various experimental techniques, periodic driving has been recognized as a key strategy for developing quantum technology. Moreover, the application of periodic driving

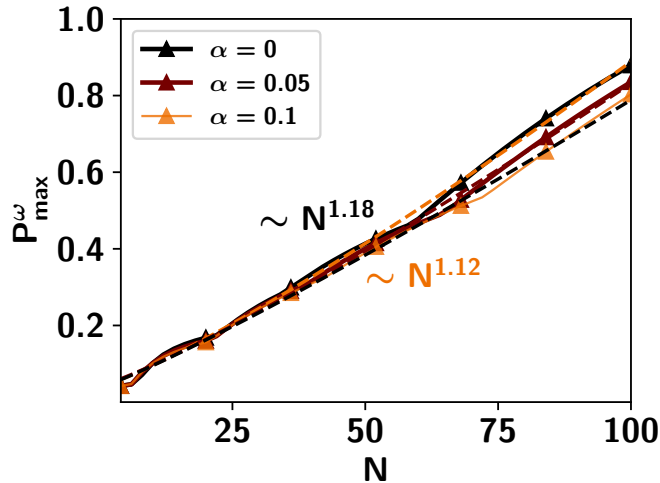


FIG. 8. **Scaling analysis for LR extended XY charging Hamiltonian.** P_{\max}^{ω} (ordinate) with system-size N (horizontal axis) for different fall-off rates α . Other parameters are $h_z = 0.02$, $J = 1$ and $\gamma = -1$. Again, by least square fitting, we find $P_{\max}^{\omega} \sim aN^{\eta} + b$ where a and b are constants and $\eta > 1$ as mentioned in the figure for low α values and $Z = N - 1$. Both the axes are dimensionless.

to quantum systems is particularly exciting due to the growing arsenal of experimental techniques, such as ultracold atoms, trapped ions, and superconducting circuits, which allow for the precise implementation of Floquet protocols. Among the various emerging quantum technologies, quantum transistors and quantum batteries (QB) stand out as two prominent areas where Floquet engineering can show significant promise.

In this study, we explored the role of Floquet evolution in enhancing the charging process of quantum batteries (QB), focusing on the maximum average power. We demonstrated that by appropriately tuning the Floquet frequency, quantum advantage can be achieved when the charging is governed by a long-range interaction Hamiltonian. Specifically, our results demonstrate that no quantum advantage exists when the system is charged using a next-nearest neighbor interacting model, even when the Floquet frequency is optimized. In contrast, when charging is governed by a long-range interacting model, a clear quantum advantage emerges in the deep long-range regime. In this regime, the power scales super-linearly with system-size. In particular, the scaling behavior depends on both the parameters of the charging Hamiltonian and the

strength of the long-range interactions, characterized by the fall-off rate. We find that as the fall-off rate increases, the scaling decreases, suggesting that weaker long-range interactions diminish the quantum advantage.

Our analysis shows that the impact of fall-off rate and the range of interactions in the scaling analysis of power is not at all straightforward. Specifically, the effect of increasing long-range interactions on the charging can be either beneficial or detrimental, depending on the specific region of the parameters under consideration. This non-monotonic behavior reflects the intricate interplay between the interaction strength, the Floquet frequency, and the underlying Hamiltonian structure.

In summary, our findings indicate that a genuine quantum advantage in the charging of quantum battery can be realized in the context of periodic driving through long-range interactions. The results also reveal the potential of periodic driving and long-range interactions as crucial tools in the development of effective quantum energy storage systems and quantum technologies, in general, emphasizing the delicate balance that must be found between system parameters to attain maximum performance.

ACKNOWLEDGMENTS

We acknowledge the use of **QIClib** – a modern C++ library for general purpose quantum information processing and quantum computing (<https://titaschanda.github.io/QIClib>), and the cluster computing facility at the Harish-Chandra Research Institute. This research was supported in part by the INFOSYS scholarship for senior students. LGCL received funds from project DYNAMITE QUANTERA2-00056 funded by the Ministry of University and Research through the ERANET COFUND QuantERA II – 2021 call and co-funded by the European Union (H2020, GA No 101017733). Funded by the European Union. Views and opinions expressed are however those of the author(s) only and do not necessarily reflect those of the European Union or the European Commission. Neither the European Union nor the granting authority can be held responsible for them. This work was supported by the Provincia Autonoma di Trento, and Q@TN, the joint lab between University of Trento, FBK—Fondazione Bruno Kessler, INFN—National Institute for Nuclear Physics, and CNR—National Research Council.

[1] R. Alicki and M. Fannes, *Phys. Rev. E* **87**, 042123 (2013).
[2] F. Campaioli, F. A. Pollock, and S. Vinjanampathy, “Quantum batteries,” in *Thermodynamics in the Quantum Regime: Fundamental Aspects and New Directions*, edited by F. Binder, L. A. Correa, C. Gogolin, J. Anders, and G. Adesso (Springer International Publishing, Cham, 2018) pp. 207–225.
[3] F. Campaioli, S. Gherardini, J. Q. Quach, M. Polini, and G. M. Andolina, *Rev. Mod. Phys.* **96**, 031001 (2024).
[4] N. Linden, S. Popescu, and P. Skrzypczyk, *Phys. Rev. Lett.* **105**, 130401 (2010).

[5] K. Joulain, J. Drevillon, Y. Ezzahri, and J. Ordonez-Miranda, *Phys. Rev. Lett.* **116**, 200601 (2016).
[6] C. M. Bender, D. C. Brody, and B. K. Meister, *Journal of Physics A: Mathematical and General* **33**, 4427 (2000).
[7] H. T. Quan, Y.-x. Liu, C. P. Sun, and F. Nori, *Phys. Rev. E* **76**, 031105 (2007).
[8] G. Gemmer, M. Michel, and G. Mahler, *Quantum Thermodynamics* (Springer, New York, 2004).
[9] J.-Y. Gyhm, D. Šafránek, and D. Rosa, *Phys. Rev. Lett.* **128**, 140501 (2022).

- [10] G. M. Andolina, V. Stanzione, V. Giovannetti, and M. Polini, “Genuine quantum advantage in non-linear bosonic quantum batteries,” (2024), [arXiv:2409.08627 \[quant-ph\]](#).
- [11] T. P. Le, J. Levensen, K. Modi, M. M. Parish, and F. A. Pollock, *Phys. Rev. A* **97**, 022106 (2018).
- [12] S. Ghosh, T. Chanda, and A. Sen(De), *Phys. Rev. A* **101**, 032115 (2020).
- [13] S. Ghosh, T. Chanda, S. Mal, and A. Sen(De), *Phys. Rev. A* **104**, 032207 (2021).
- [14] S. Ghosh and A. Sen(De), *Phys. Rev. A* **105**, 022628 (2022).
- [15] S. Julià-Farré, T. Salamon, A. Riera, M. N. Bera, and M. Lewenstein, *Phys. Rev. Res.* **2**, 023113 (2020).
- [16] D. Ferraro, M. Campisi, G. M. Andolina, V. Pellegrini, and M. Polini, *Phys. Rev. Lett.* **120**, 117702 (2018).
- [17] G. M. Andolina, M. Keck, A. Mari, V. Giovannetti, and M. Polini, *Phys. Rev. B* **99**, 205437 (2019).
- [18] A. C. Santos, B. i. e. i. f. m. c. Çakmak, S. Campbell, and N. T. Zinner, *Phys. Rev. E* **100**, 032107 (2019).
- [19] D. Rossini, G. M. Andolina, D. Rosa, M. Carrega, and M. Polini, *Phys. Rev. Lett.* **125**, 236402 (2020).
- [20] K. Sen and U. Sen, *Phys. Rev. A* **104**, L030402 (2021).
- [21] A. Crescente, M. Carrega, M. Sassetti, and D. Ferraro, *Phys. Rev. B* **102**, 245407 (2020).
- [22] A. Crescente, D. Ferraro, M. Carrega, and M. Sassetti, *Phys. Rev. Res.* **4**, 033216 (2022).
- [23] T. K. Konar, L. G. C. Lakkaraju, S. Ghosh, and A. Sen(De), *Phys. Rev. A* **106**, 022618 (2022).
- [24] T. K. Konar, A. Patra, R. Gupta, S. Ghosh, and A. Sen(De), *Phys. Rev. A* **110**, 022226 (2024).
- [25] T. K. Konar, L. G. C. Lakkaraju, and A. Sen (De), *Phys. Rev. A* **109**, 042207 (2024).
- [26] P. Chaki, A. Bhattacharyya, K. Sen, and U. Sen, [arXiv \(2024\)](#), 10.48550/arXiv.2404.18745, 2404.18745.
- [27] M. B. Arjmandi, A. Shokri, E. Faizi, and H. Mohammadi, *Phys. Rev. A* **106**, 062609 (2022).
- [28] T. F. F. Santos, Y. V. de Almeida, and M. F. Santos, *Phys. Rev. A* **107**, 032203 (2023).
- [29] P. Chaki, A. Bhattacharyya, K. Sen, and U. Sen, [arXiv \(2023\)](#), 10.48550/arXiv.2307.16856, 2307.16856.
- [30] C. Rodríguez, D. Rosa, and J. Olle, *Phys. Rev. A* **108**, 042618 (2023).
- [31] A. Mitra and S. C. L. Srivastava, *Phys. Rev. A* **110**, 012227 (2024).
- [32] J.-s. Yan and J. Jing, *Phys. Rev. Appl.* **19**, 064069 (2023).
- [33] W.-L. Song, H.-B. Liu, B. Zhou, W.-L. Yang, and J.-H. An, *Phys. Rev. Lett.* **132**, 090401 (2024).
- [34] Z.-G. Lu, G. Tian, X.-Y. Lü, and C. Shang, “Topological quantum batteries,” (2024), [arXiv:2405.03675 \[quant-ph\]](#).
- [35] Z. Niu, Y. Wu, Y. Wang, X. Rong, and J. Du, *Phys. Rev. Lett.* **133**, 180401 (2024).
- [36] A. Mitra and S. C. L. Srivastava, “Ergotropy, bound energy and entanglement in 1d long range kitaev model,” (2024), [arXiv:2408.05063 \[cond-mat.str-el\]](#).
- [37] F. Percivalle, D. Rossini, J. Polo, and L. Amico, “Extractable energy from quantum superposition of current states,” (2024), [arXiv:2410.13934 \[quant-ph\]](#).
- [38] G. Zhu, Y. Chen, Y. Hasegawa, and P. Xue, *Phys. Rev. Lett.* **131**, 240401 (2023).
- [39] D. Rossini, G. M. Andolina, and M. Polini, *Phys. Rev. B* **100**, 115142 (2019).
- [40] M. B. Arjmandi, H. Mohammadi, A. Saguia, M. S. Sarandy, and A. C. Santos, *Phys. Rev. E* **108**, 064106 (2023).
- [41] I. M. de Buy Wenniger, S. E. Thomas, M. Maffei, S. C. Wein, M. Pont, N. Belabas, S. Prasad, A. Harouri, A. Lemaître, I. Sagnes, N. Somaschi, A. Auffèves, and P. Senellart, “Experimental analysis of energy transfers between a quantum emitter and light fields,” (2023), [arXiv:2202.01109 \[quant-ph\]](#).
- [42] F.-Q. Dou and F.-M. Yang, *Phys. Rev. A* **107**, 023725 (2023).
- [43] C.-K. Hu, J. Qiu, P. J. P. Souza, J. Yuan, Y. Zhou, L. Zhang, J. Chu, X. Pan, L. Hu, J. Li, Y. Xu, Y. Zhong, S. Liu, F. Yan, D. Tan, R. Bachelard, C. J. Villas-Boas, A. C. Santos, and D. Yu, *Quantum Science and Technology* **7**, 045018 (2022).
- [44] G. Gemme, M. Grossi, D. Ferraro, S. Vallecorsa, and M. Sassetti, *Batteries* **8** (2022), 10.3390/batteries8050043.
- [45] J. Q. Quach, K. E. McGhee, L. Ganzer, D. M. Rouse, B. W. Lovett, E. M. Gauger, J. Keeling, G. Cerullo, D. G. Lidzey, and T. Virgili, *Sci. Adv.* **8** (2022), 10.1126/sciadv.abk3160.
- [46] J. Joshi and T. S. Mahesh, *Phys. Rev. A* **106**, 042601 (2022).
- [47] M. Bukov, L. D’Alessio, and A. Polkovnikov, *Adv. Phys.* (2015).
- [48] A. Eckardt and E. Anisimovas, *New J. Phys.* **17**, 093039 (2015).
- [49] T. Mori, *Annu. Rev. Condens. Matter Phys.* , 35 (2023).
- [50] A. J. McRoberts, H. Zhao, R. Moessner, and M. Bukov, *Phys. Rev. Res.* **5**, 043008 (2023).
- [51] L. D’Alessio, Y. Kafri, A. Polkovnikov, and M. Rigol, in *AIP Conference Proceedings* (AIP Publishing, 2016).
- [52] I. Bloch, J. Dalibard, and W. Zwerger, *Rev. Mod. Phys.* **80**, 885 (2008).
- [53] M. Aidelsburger, M. Atala, M. Lohse, J. T. Barreiro, B. Paredes, and I. Bloch, *Phys. Rev. Lett.* **111**, 185301 (2013).
- [54] A. Eckardt, *Rev. Mod. Phys.* **89**, 011004 (2017).
- [55] G. Engelhardt, S. Choudhury, and W. V. Liu, *Phys. Rev. Res.* **6**, 013116 (2024).
- [56] B. Fauseweh and J.-X. Zhu, *Quantum* **7**, 1063 (2023).
- [57] D. Kolisnyk, F. Queißer, G. Schaller, and R. Schützhold, *Phys. Rev. Appl.* **21**, 044050 (2024).
- [58] N. Gupt, S. Bhattacharyya, B. Das, S. Datta, V. Mukherjee, and A. Ghosh, *Phys. Rev. E* **106**, 024110 (2022).
- [59] W. Niedenzu, D. Gelbwaser-Klimovsky, and G. Kurizki, *Phys. Rev. E* **92**, 042123 (2015).
- [60] W. Niedenzu and G. Kurizki, *New J. Phys.* **20**, 113038 (2018).
- [61] S. Mondal and S. Bhattacharjee, *Phys. Rev. E* **105**, 044125 (2022).
- [62] T. Koffel, M. Lewenstein, and L. Tagliacozzo, *Phys. Rev. Lett.* **109**, 267203 (2012).
- [63] D. Vodola, L. Lepori, E. Ercolessi, A. V. Gorshkov, and G. Pupillo, *Phys. Rev. Lett.* **113**, 156402 (2014).
- [64] C. Mahto, V. Pathak, A. K. S., and A. Shaji, *Phys. Rev. A* **106**, 012427 (2022).
- [65] Monika, L. G. C. Lakkaraju, S. Ghosh, and A. S. De, “Better sensing with variable-range interactions,” (2023), [arXiv:2307.06901 \[quant-ph\]](#).
- [66] D. Ghosh, K. Das Agarwal, P. Halder, and A. Sen(De), *Phys. Rev. A* **110**, 022431 (2024).
- [67] Y. Wang, M. Um, J. Zhang, S. An, M. Lyu, J.-N. Zhang, L.-M. Duan, D. Yum, and K. Kim, *Nat. Photonics* **11**, 646 (2017).
- [68] S. Olmschenk, K. C. Younge, D. L. Moehring, D. N. Matsukevich, P. Maunz, and C. Monroe, *Phys. Rev. A* **76**, 052314 (2007).
- [69] R. He, M.-Z. Ai, J.-M. Cui, Y.-F. Huang, Y.-J. Han, C.-F. Li, G.-C. Guo, G. Sierra, and C. E. Creffield, *npj Quantum Inf.* **7**, 1 (2021).
- [70] E. Lieb, T. Schultz, and D. Mattis, *Annals of Physics* **16**, 407 (1961).
- [71] E. Barouch, B. M. McCoy, and M. Dresden, *Phys. Rev. A* **2**, 1075 (1970).
- [72] E. Barouch and B. M. McCoy, *Phys. Rev. A* **3**, 786 (1971).

- [73] D. Vodola, L. Lepori, E. Ercolessi, and G. Pupillo, *New Journal of Physics* **18**, 015001 (2015).
- [74] D. Sadhukhan, A. Sinha, A. Francuz, J. Stefaniak, M. M. Rams, J. Dziarmaga, and W. H. Zurek, *Phys. Rev. B* **101**, 144429 (2020).
- [75] D. Jaschke, K. Maeda, J. D. Whalen, M. L. Wall, and L. D. Carr, *New Journal of Physics* **19**, 033032 (2017).
- [76] L. G. C. Lakkaraju, S. Ghosh, D. Sadhukhan, and A. Sen(De), *Phys. Rev. A* **106**, 052425 (2022).
- [77] H. Lipkin, N. Meshkov, and A. Glick, *Nuclear Physics* **62**, 188 (1965).
- [78] M. N. Bera, A. Riera, M. Lewenstein, Z. B. Khanian, and A. Winter, *Quantum* **3**, 121 (2019).
- [79] M. Kac, G. E. Uhlenbeck, and P. C. Hemmer, *J. Math. Phys.* **4**, 216 (1963).
- [80] M. A. Nielsen and I. L. Chuang, *Quantum Computation and Quantum Information*, 1st ed. (Cambridge University Press, Cambridge, UK, 2000).
- [81] V. Giovannetti, S. Lloyd, and L. Maccone, *Phys. Rev. Lett.* **96**, 010401 (2006).
- [82] A. S. De and U. Sen, “Quantum advantage in communication networks,” (2011), arXiv:1105.2412 [quant-ph].
- [83] N. Gisin and R. Thew, *Nature Photonics* **1**, 165–171 (2007).
- [84] S. Blanes, F. Casas, J. Oteo, and J. Ros, *Physics Reports* **470**, 151 (2009).
- [85] W. Magnus, *Communications on Pure and Applied Mathematics* **7**, 649 (1954).
- [86] F.-Q. Dou, Y.-J. Wang, and J.-A. Sun, “Charging advantages of lipkin-meshkov-glick quantum battery,” (2022), arXiv:2208.04831 [quant-ph].
- [87] S. Dusuel and J. Vidal, *Phys. Rev. Lett.* **93**, 237204 (2004).
- [88] J. Vidal, G. Palacios, and C. Aslangul, *Phys. Rev. A* **70**, 062304 (2004).
- [89] S. Dusuel and J. Vidal, *Phys. Rev. B* **71**, 224420 (2005).
- [90] L. G. C. Lakkaraju, S. Ghosh, S. Roy, and A. Sen(De), *Physics Letters A* **418**, 127703 (2021).
- [91] G. B. Mbeng, A. Russomanno, and G. E. Santoro, *SciPost Phys. Lect. Notes* , 82 (2024).